Proceedings of the 13th International Symposium on Experimental Computational Aerothermodynamics of Internal Flows
7–11 May 2017, Okinawa, Japan

ISAIF13-S-0090

Numerical Approach Dedicated to Nozzle Tip Clearance Flow Analysis in Variable Geometry Radial Turbines

P. T. Lauriau[1,2], N. Binder[2], X. Carbonneau[2], S. Cros[1], M. Roumeas[1]

1 Research & Expertise Department, Liebherr Aerospace Toulouse (LTS).
Avenue des Etats-Unis, 408, 31016, Toulouse, France.
pierrethomas.lauriau@liebherr.com
sandrine.cros@liebherr.com
mathieu.roumeas@liebherr.com

2 Institut Supérieur de l'Aéronautique et de l'Espace (ISAE SUPAERO), Université de Toulouse.
Avenue Edouard Belin, 10, 31400, Toulouse, France.
pierre-thomas.lauriau@isae.fr
nicolas.binder@isae.fr
xavier.carbonneau@isae.fr

Abstract

The present paper consists in a numerical analysis of a variable geometry radial turbine stage, for three opening configurations. The presence of the endwall clearance in the stator creates additional secondary flows upstream from the rotor, which tend to increase the stator–rotor interactions. Those interactions are filtered in steady-state simulations, for which the accuracy is expected to decrease. A comparison between steady-state mixing plane simulations and a Non Linear Harmonic (NLH) approach is thus proposed, together with an analysis of the influence of the numbers of harmonics chosen for the NLH simulations. The results show that the implementation of clearances in the simulations increases the discrepancies between the two methods, especially for configurations naturally sensitive to stator–rotor interactions (open stator configuration). Regarding the number of harmonics for the numerical setting, a criterion proposed in the literature is discussed at the end of the paper, and provides good guidelines in order to avoid a full harmonics convergence analysis.

Keywords: Radial Inflow Turbines, Variable Geometry Radial Turbines, Off–Design, Non Linear Harmonic Methods, Tip Clearance Flows.

Introduction

Variable nozzle radial turbines are widely used for various applications such as automotive turbochargers and aeronautic air conditioning systems. The wider operating range provided by the variable geometry device allows the development of new architectures of Environmental Control Systems manufactured by Liebherr Aerospace (LTS), where the turbine is designed from a multi-points specification: the radial turbine efficiency has to be acceptable for a large range of operating points. But the off-design operation of the rotor is associated to a drop of the performances [1, 2]. Moreover, designers have to deal with a nozzle endwall clearance which is necessary for the rotation of the nozzle vanes. It is well-known that this endwall clearance affects the flow field in the whole turbine stage, and leads to an additional efficiency penalty as shown in [3, 4]. The highly 3D complex topology of the flow field in a variable nozzle radial turbine is well characterized in the literature [5], as well as secondary flows which induce some losses of the turbine stage. Among them, one can find some classical vortices such as horseshoe vortex and corner vortex (see [6, 7]). In case of variable geometry turbines, the nozzle leakage vortex generated through the interaction between the nozzle leakage flow and the main flow is considered as the dominant secondary flow coming from the stator. Some aerodynamic descriptions of this secondary flow structure are proposed in [8–10]. This nozzle leakage vortex is found to affect the main flow characteristics especially through the decrease of both the stator aerodynamic throat [11] and the stator outlet flow angle [12]. Furthermore, as shown in [11, 13], it interacts with others secondary flows such as stator vane wakes and it can modify the topology of the shock which happens near the stator trailing edge for stator transonic conditions. These interactions are responsible for the turbine efficiency drop through an entropy production in the stage. Also, they are directly related to nozzle vane loading which determines the nozzle tip-leakage flow intensity. Hence, the global performance of the stage is also affected by the nozzle endwall clearance position (hub, shroud, or divided between both sidewall), depending on the stator opening configuration (see [12, 14, 15]).
3D RANS mixing-plane simulations restricted to one passage per row are convenient to investigate such a com-

plex flow through numerical simulations for a relatively low cost, as found in [5, 14]. Though, the azimuthal averaging applied by the mixing plane at the interface filters the stator–rotor interaction. Some Fourier methods (temporal or spatial) can be considered to perform quasi-unsteady calculations taking into account the first order stator–rotor interaction. The calculation is still restricted to one blade passage through the phase-lagged technique. A description of these Fourier-based time integration approaches is brought in [16]. In the present paper, Non-Linear Harmonic (NLH) methods implemented into FINE/Turbo from NUMECA are used. This implementation is described in [17], together with an application to a radial turbine. To date, this NLH approach is largely validated in the open literature for a large range of applications (see [18]). In addition, recent works [19] have applied this NLH method to a variable geometry radial turbine in order to characterize the unsteady radial load due to the circumferential mode 1. Though, the nozzle endwall clearance is not taken into account in the model.

As the flow topology in a turbine stage directly depends on both the geometry (stator opening) and the operating point, secondary flow topologies which cross the stator–rotor interface (nozzle leakage flow, nozzle vane wakes, etc.) vary as well with the stator opening configuration. This directly modifies the stator–rotor interaction [20]. Then, the simulation requires the adequate setting for the number of harmonics: a higher number of harmonics provides a better continuity of the unsteady flow across the interface, but for a higher cost (which remains low compared to standard unsteady methods). This setting is problem–dependent (as noted in [21]), and must be considered as well as the mesh dependence. Intuitively, one can expect a higher required number of harmonics for topologies with higher flow spatial gradients. The harmonic convergence for Fourier-based methods is tackled especially in [17, 21] with a frequency-domain approach (NLH), and for instance in [22] with a time-domain harmonic balance approach. These studies are dedicated to various turbomachinery applications and lead to different required numbers of harmonics. Still with a time-domain approach, a consensus is then proposed in [23], through a criterion for the minimal number of harmonics required to achieve a specified accuracy level. Thus, the authors propose an approach based on an azimuthal Fourier transform performed at the rows interface in a mixing plane computation. This criterion takes into account spatial distortions induced for instance by viscosity effects near walls and tip vortex, and is applied to contra-rotating open rotor simulations.

In case of variable geometry radial turbines, the flow crossing the interface is distorted especially near walls because of nozzle endwall clearance effects. Those effects can be fed to the rotor thanks to the frequency-domain approach NLH, and might lead to significant discrepancies with regard to classical steady-state mixing plane results. Hence, this paper intends to compare results coming from steady-state mixing plane and Non Linear Harmonic computations, for three typical operating points of a radial turbine stage from LTS:

- the nominal operating point;
- a highly loaded case with a closed stator position;
- a lowly loaded case with a full open stator position;

The first part of this paper focuses on the description of the numerical set up considered and the test cases. More specifically, steady-state mixing plane and NLH approaches are discussed. Afterwards, these methodologies are compared for the three specified operating points, with the nozzle endwall clearances. The choice of the numerical methodology to investigate the turbine stage behaviour with or without nozzle endwall clearance is then discussed, together with the number of harmonics for NLH computations with regard to the criterion brought in [23].

Numerical Procedure

Numerical Model and Test Cases

The computational domain investigated in this paper is reduced to a single blade passage of both the stator and the rotor. The volute scroll upstream the nozzle is not taken into account to save computational resources. Figure 1 shows a meridional view of the turbine stage and the extraction planes considered in this paper to compute the turbine performances and to characterize the flow topology:

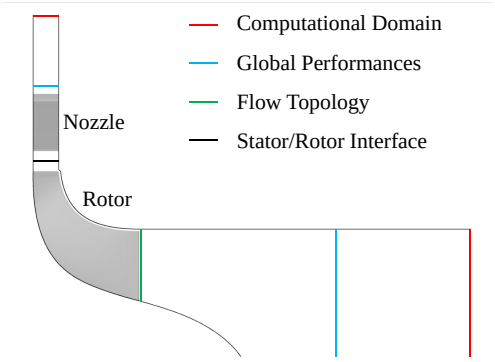

Figure 1 Meridional view of the radial turbine stage with extraction planes considered for the study.

A nozzle endwall clearance, typical of variable opening stages, represents 2.4% of the stator vane height. This clearance is divided equally between the hub and the tip. The rotor inlet diameter is around 150 mm, and a constant rotor tip clearance of 0.65 mm is implemented in the numerical model. As explained above, three typical operating points are numerically investigated, for which both the nozzle opening and the stage loading are different. The main specifications are presented in Table 1.

Flow Solver

The flow solver EURANUS is integrated in the commercial CFD solver FINE/Turbo from NUMECA. It is a 3D

Table 1 Main characteristics of the test cases: nozzle opening configurations and associated operating points.

Stator opening configuration	Nominal	Closed	Open
Hub clearance (% Vane height)		1.2	
Tip clearance (% Vane height)		1.2	
α_{metal} at nozzle outlet (°)	77.9	84.3	58.7
Stator–rotor radial gap (mm)	6.5	8.3	0.9
Total-to-static pressure ratio	3.26	4	1.56
Rotational speed (RPM)	47000	41600	32700
Isentropic velocity ratio	0.7	0.6	0.8

density-based code, which solves the steady and unsteady Reynolds Averaged Navier Stokes equations based on a finite volume method. In this study, steady and Non Linear Harmonic simulations have been performed. For both cases, a second order central difference scheme is employed for the spatial discretization, with Jameson type artificial dissipation. A four-stage explicit Rouge-Kutta scheme is applied for the temporal discretization. For steady calculations, the equations are advanced in pseudo time. To speed up the calculations convergence, the multigrid method is used and combined with a local time-stepping and an implicit residual smoothing. The chosen turbulence model is the Spalart-Allmaras model. Also, the fluid (air) is modelled through a perfect gas equation with variable heat capacity and variable laminar dynamic viscosity through the Sutherland's law. For NLH computations, one perturbation is solved in each row and different harmonic values are used per perturbation. For both the nominal point and the closed stator case, a range of 1 to 6 harmonics is investigated. For the open stator configuration, NLH computations are performed from 2 to 6 harmonics (no convergence was reached with the number of harmonics set to 1 for this configuration).

Meshing Considerations

The structured mesh is generated using AutoGrid from NUMECA. The grid topology is composed of H, C and O blocks. The mesh inside a clearance is created using the butterfly topology: an H block is surrounded by an O block to discretize the clearance domain. 41 points are used to discretize the clearance gaps in the spanwise direction. The size of the first cell in the normal direction at the wall is equal to 1 micrometer and ensures that y^+ are strictly lower than 5 at the hub, shroud and vane/blade walls. The stator and the rotor mesh sizes are respectively 5.5 and 4.8 million points. A mesh sensitivity analysis showed that this configuration was the best trade-off between local flow filed convergence and computational cost. Also, this mesh fulfils the azimuthal discretization criteria required by the NLH approach.

Boundary Conditions

At the inlet of the computational domain, total pressure, total temperature and flow angles are uniformly prescribed. The inlet flow angle is estimated from a typical volute geometry; a value of 63° is applied. At the outlet, a static pressure value is imposed. Adiabatic conditions are applied to the hub, blade surfaces and casing. An azimuthal periodicity of the single passage is applied for steady cases, while a spatio-temporal periodicity is considered for NLH calculations. The interface between the rotor and the stator is treated with a non-reflecting 1D mixing-plane approach for steady calculations, while complex non-reflecting boundary conditions using phase-lagged decomposition are used for NLH calculations.

Comparison of Numerical and Experimental Results

The nature of this work is essentially numerical, to analyze the sensitivity of the simulation to the numerical setting. Anyway, the finality of this work is focused on physical analysis, for which a formal validation is required. A test bench is currently developed in that purpose, which gave preliminary results for configurations without end-wall clearances. A comparison with those preliminary results is thus proposed, in order to check the relevance of the simulations for both mixing plane and NLH methods. Table 2 details this geometric configuration as well as the operating point. The total-to-static efficiency measurement process still needs to be secured, and is just given for information. It cannot be considered as a strong validation indicator, especially since in the experiment, the volute losses are integrated. The mass-flow measurement is more consolidated. All the simulations predict accurately this indicator (see Table 3).

Table 2 Experimental data – operating point.

Stator opening configuration	Nominal
Hub clearance (% Vane height)	0
Tip clearance (% Vane height)	0
Total-to-static pressure ratio	2.5
Corrected rotational speed (RPM)	38150
Isentropic velocity ratio	0.65

Table 3 Evaluation of both numerical approaches.

Computation	ΔCorr. MFR (%) compared with expe.	ΔEfficiency (points) compared with expe.
Steady-state mixing plane	$+1.4$	$+3$
NLH with 1 harmonic	$+0.4$	$+5.3$
NLH with 2 harmonics	$+0.4$	$+5$
NLH with 3 harmonics	$+0.4$	$+5$

Global Performances

The global performances reached by the radial turbine stage for the three presented operating points are shown in Tables 4, 5 and 6. These results are extracted from time-averaged solutions of NLH computations (from 1 to 6 harmonics), and also from steady-state mixing plane computations (0 harmonic). For each operating point, values indicated in Tables 4 to 6 are relative to results obtained for the most expensive computation (Non Linear Harmonic with 6 harmonics). If the convergence is reached before 6 harmonics; the last results are omitted in the Tables.

Table 4 Influence of the number of harmonics on the global performances for the nominal operating point.

Number of harmonics	ΔMFR (%) compared with NLH–6 harmonics	ΔEfficiency (points) compared with NLH–6 harmonics
0	+ 2	− 0.7
1	+ 0.1	+ 0.1
2	0	+ 0.1
3	0	0

Table 5 Influence of the number of harmonics on the global performances for the closed stator case.

Number of harmonics	ΔMFR (%) compared with NLH–6 harmonics	ΔEfficiency (points) compared with NLH–6 harmonics
0	+ 1.1	+ 0.28
1	+ 0.1	+ 0.3
2	+ 0.2	+ 0.35
3	+ 0.2	+ 0.33
4	0	0

Table 6 Influence of the number of harmonics on the global performances for the open stator case.

Number of harmonics	ΔMFR (%) compared with NLH–6 harmonics	ΔEfficiency (points) compared with NLH–6 harmonics
0	+ 3.5	− 3.6
2	+ 0.8	− 0.3
3	+ 0.4	− 0.2
4	+ 0.1	− 0.1
5	0	0

The analysis of the global indicators shows that the discrepancies between mixing-plane and NLH simulations do not exceed 4% for the mass-flow and 4 points for the total-to-static efficiency. The opening configuration has a clear influence, and can be correlated to the degree of unsteadiness expected: high in the open configuration because of a very small radial distance between rotor and stator (see Table 1), and much smaller in the closed configuration for which a mixing process occurs upstream the stator–rotor interface. Also, the number of harmonics does not have a strong influence on the global indicators for all cases. It means that the essential of the difference between the two methods can be captured with a single harmonic calculation. It is noteworthy that the difference between mixing-plane and NLH simulations increases with the presence of stator endwall clearances (see Tables 3 & 4).
These results might be explained by the nature of the stator–rotor interaction which varies and is determined by the geometry configuration (see Table 1). The flow topologies are then investigated in the following sections, and the influence of the number of harmonics is characterized with reference to local flow criteria.

Nominal Operating Point

The following analysis aims at the description of the local flow provided by the 6 harmonics numerical simulation. It still needs a formal experimental validation which is under way, but is interesting from the numerical point of view since the influence of the number of harmonics on the flow physics is highlighted. That is why the flow structures met for the three operating points are synthesized without going in much details, especially for secondary flows already characterized in the open literature.

Main Secondary Flow Structures

With reference to the nominal point, some instantaneous blade-to-blade entropy contours coming from a NLH computation are presented in Figures 2 and 3.

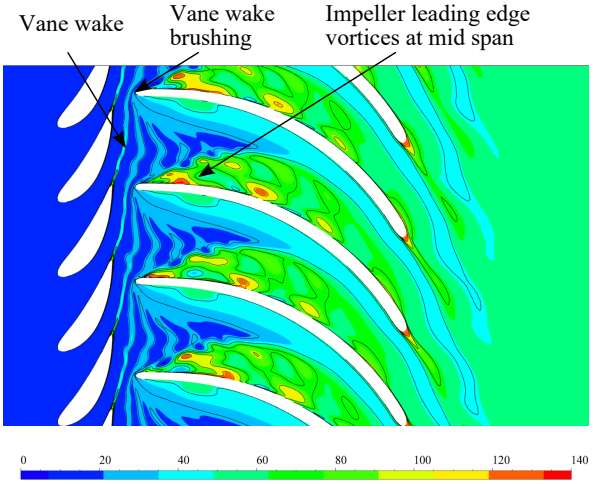

Figure 2 Blade-to-blade entropy contour for the nominal operating point at 50% span.

As illustrated by these Figures, the main mechanisms leading to entropy creation are:

- A brushing of the stator vane wakes by the impeller leading edge (Figure 2). This mechanism happens on the whole span except close to the walls.
- Close to the walls (Figures 3), the nozzle leakage vortex interacts with the adjacent nozzle vane wake.

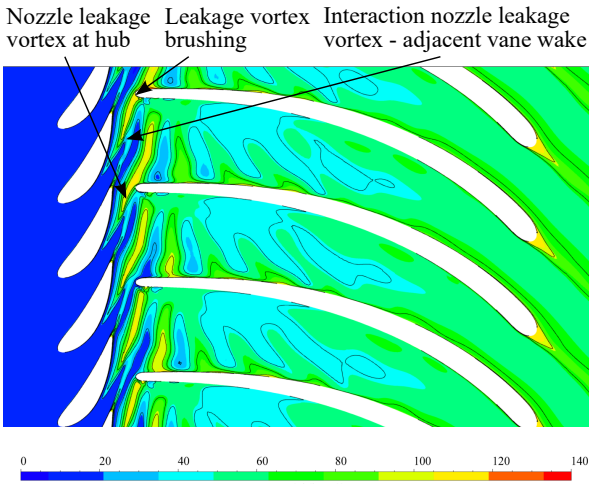

Figure 3 Blade-to-blade entropy contour for the nominal operating point at 10% span.

This interaction happens downstream to the interface. These structures are also brushed by the impeller leading edge.

- At mid-span (Figure 2), an entropy rise is noticeable in the rotor passage at the suction side from the leading edge to the trailing edge. It is due to the generation of two vortices at midspan of the impeller leading edge, which were already observed in [24].

Influence of the Number of Harmonics on the Flow Field

The above entropy contours are obtained through a NLH computation with 6 harmonics. Figure 4 shows the time and pitch averaged absolute angle extracted at rotor exit, in order to check the influence of the number of harmonics on the local flow field:

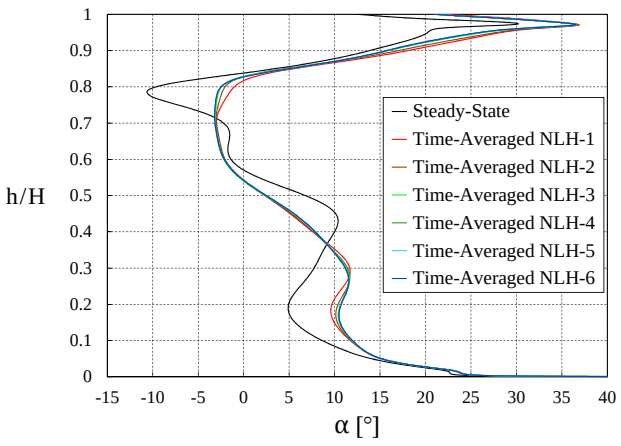

Figure 4 Evolution of the time and pitch averaged swirl at rotor exit from hub to shroud – Nominal operating point.

This analysis is relevant as the outlet profile is affected by the complex interactions arising in the whole turbine stage. Hence, the absolute angle distribution is distorted over the span. These distortions seem overestimated by the steady mixing-plane results compared to NLH time-averaged results, even if the trend is well caught for the rotor tip leakage vortex (from 90 to 100% of the spanwise direction). With regard to the number of harmonics, no evolution is observed from 4 to 6 harmonics, and an excellent trend is obtained with 3 harmonics. This confirms observations related to Table 4.

Regarding the transmission of information at the interface, some instantaneous entropy signals are extracted upstream and downstream the stator–rotor interface close to the hub (Figure 5). These entropy signals are plotted over a pitch range of 70°. On each graph, one can distinguish a main entropy pic corresponding to the nozzle leakage vortex crossing the interface, and a secondary peak corresponding to the nozzle vane wake. For this simple case with two distinct main peaks, a very good trade-off is obtained with 4 harmonics. Indeed, amplitudes of the signal are well reproduced at the interface outlet, and no major evolution occurs with a higher number of harmonics (5 or 6). Some equivalents conclusions can be brought for others spanwise position such as 50% and 90%. We will see that this is not necessarily the case for the two off-design configurations (see Table 1) presented in the following sections.

Closed Stator Case

Main Secondary Flow Structures

The highly loaded case with a closed nozzle configuration is firstly investigated. Instantaneous blade-to-blade contours from a 6 harmonics NLH computation are considered to specify the flow field (Figures 6, 7 and 8).

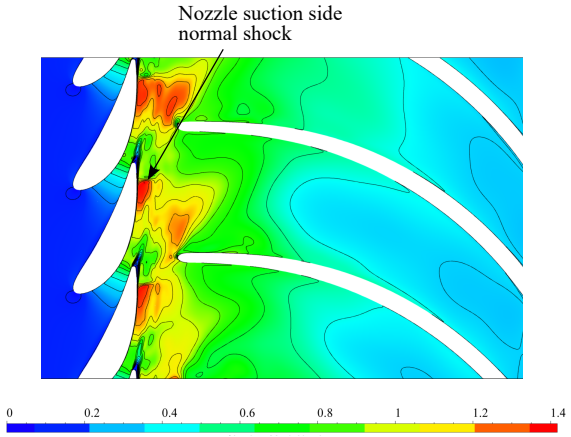

Figure 6 Blade-to-blade absolute Mach number contour for the closed stator case at 50% span.

These Figures highlight the following mechanisms:

- The high total-to-static pressure ratio (equal to 4) leads to transonic conditions at the nozzle outlet, as shown in Figure 6. A normal shock occurs close to the nozzle trailing edge at the suction side. Its inten-

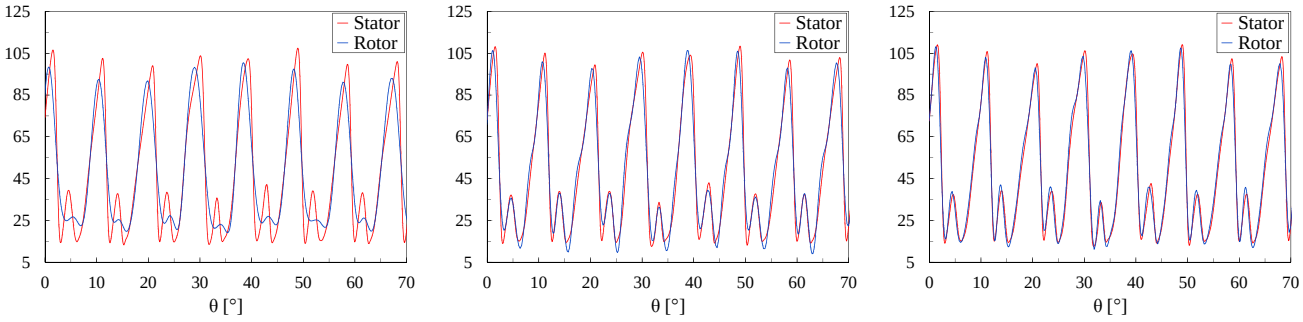

(a) 2 Harmonics (b) 3 Harmonics (c) 4 Harmonics

Figure 5 Entropy signal ($J.kg^{-1}.K^{-1}$) at the interface for the nominal operating point – 10% span.

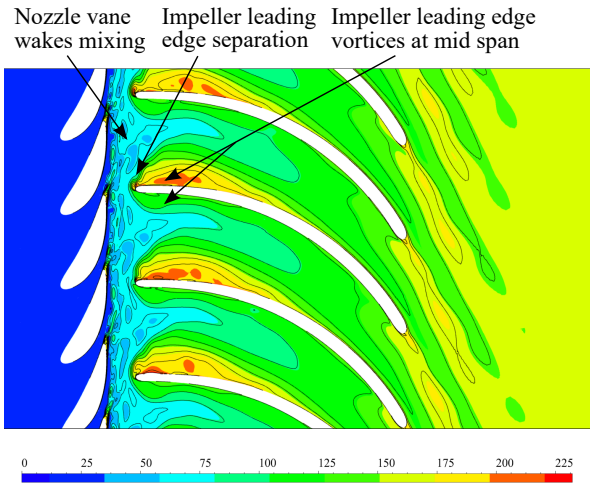

Figure 7 Blade-to-blade entropy contour for the closed stator case at 50% span.

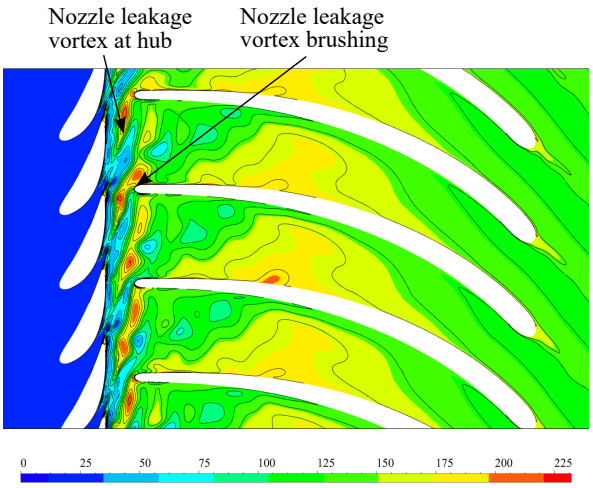

Figure 8 Blade-to-blade entropy contour for the closed stator case at 10% span.

sity varies because of static pressure periodic fluctuations due to rotor blades passage in front of the nozzle vane.

- At 50% span, the rotor is not adapted to the flow coming from the nozzle. Indeed the mean relative angle of the fluid at the impeller inlet is 9°, while the rotor is designed from the well know ideal range [-20°; -40°]. Hence, a massive leading edge separation happens on the suction side.
- At 10% span (respectively at 90% span), a nozzle leakage vortex is generated at the suction side from the first half cord of the vane because of the high blade loading. This leakage vortex interacts with the adjacent vane wake upstream the interface. This incoming flow is then brushed by the impeller leading edge.
- Close to the walls, the impeller leading edge separation is reduced because of nozzle leakage flow and boundary layers effects: the mean relative angle of the fluid is reduced at the impeller inlet.

Furthermore, because of the high vane opening angle and the relatively large radial gap (8.3 mm) between the stator trailing edge and the rotor leading edge, vane wakes interact with each other and a mixing process is naturally carried out in the free space. This mixing happens in the whole span excepted close to the walls. Thus a classical steady-state mixing plane seems particularly adapted for this topology. This explains in particular why steady-state results from Table 5 are closer to NLH results for this operating point.

Influence of the Number of Harmonics on the Flow Field

The previous blade-to-blade contours arise from an instantaneous 6 harmonics NLH solution. The time and pitch averaged flow is firstly considered to characterize the influence of the number of harmonics for this highly loaded functioning point (see Figure 9). The trend for the absolute flow angle at the rotor exit is relatively well caught by the steady-state result with reference to time-averaged NLH results. From 4 to 6 harmonics time-averaged results, no evolution is observed. This value of 4 harmonics has already been highlighted trough observations related to Table 5 for this operating point.

Let us now consider some instantaneous entropy signals extracted at the interface close to the hub (Figure 10). These signals are more complex with reference to the nominal case, because of mechanisms discussed above. Both

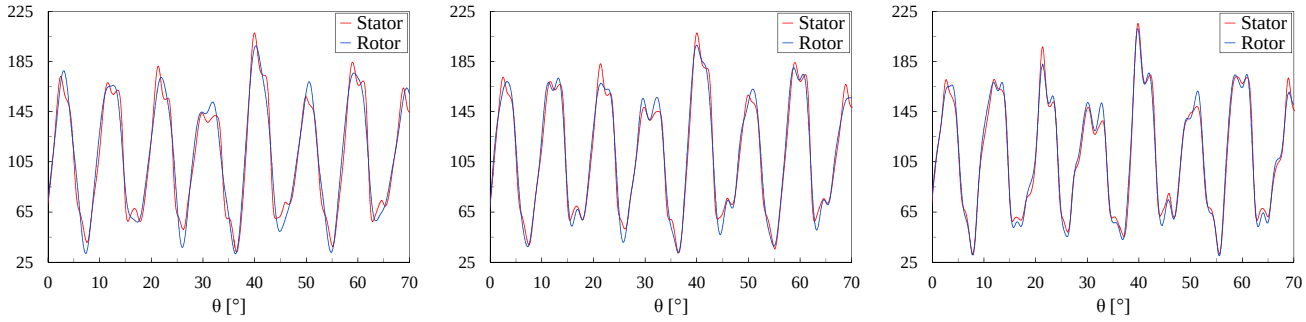

(a) 2 Harmonics (b) 3 Harmonics (c) 4 Harmonics

Figure 10 Entropy signal ($J.kg^{-1}.K^{-1}$) at the interface for the closed stator case – 10% span.

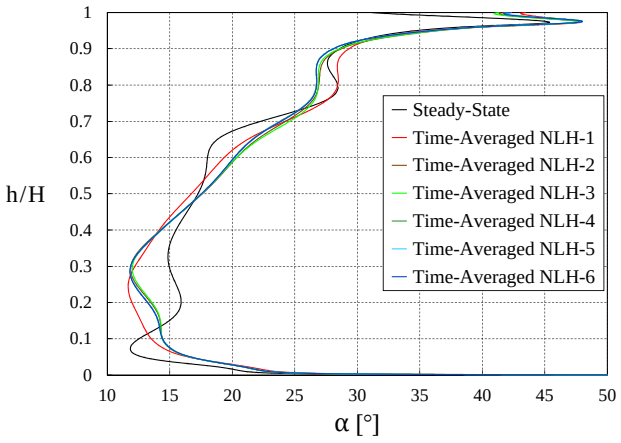

Figure 9 Evolution of the time and pitch averaged swirl at rotor exit from hub to shroud – Closed stator case.

stator and rotor entropy signals match relatively well starting from 4 harmonics, and a higher number of harmonics (5 or 6) does not reduce the discrepancies neither modifies the signal topology. Some similar observations arise from 50% and 90% spanwise positions. Thus a 4 harmonic NLH computation seems to be a good trade-off. Although, this result might vary for another off-design operating point, especially for an open stator configuration.

Open Stator Case

Main Secondary Flow Structures

The third operating point studied is the lowly loaded case with a full open stator configuration. Instantaneous blade-to-blade entropy contours from a 6 harmonics NLH computation are presented in Figures 11 and 12. For this configuration, the main mechanisms leading to entropy creation are:

- At nozzle vane inlet, the modification of the vane angle entails a leading edge separation. The flow does not reattach before the trailing edge and a large vane wake is induced.
- The rotor is not adapted to the flow coming from the nozzle because of a very negative mean relative angle of the fluid at the impeller inlet (-55°).

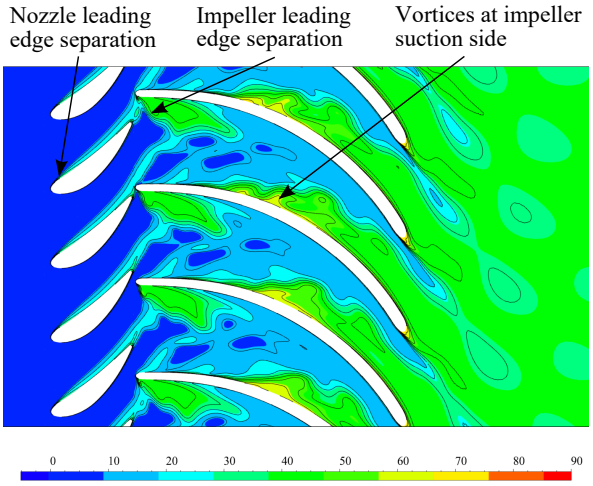

Figure 11 Blade-to-blade entropy contour for the open stator case at 50% span.

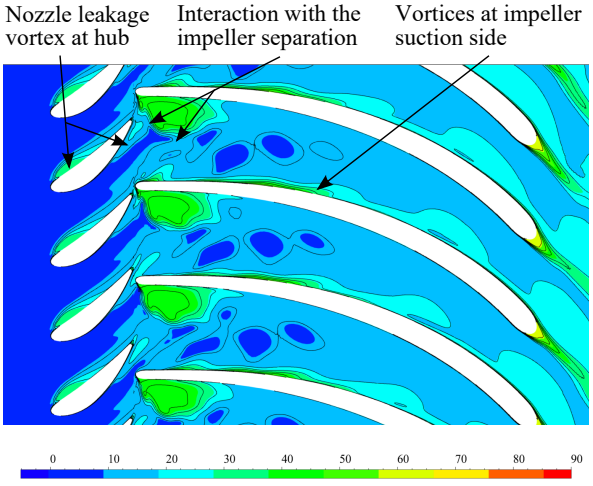

Figure 12 Blade-to-blade entropy contour for the open stator case at 10% span.

- The vane wakes are brushed by the impeller leading edge and impact the leading separation generated at the rotor pressure side.

- Near the walls, nozzle leakage vortices are generated and interact with mechanisms previously mentioned. Moreover, the impeller leading edge separation is larger because of leakage vortex and boundary layers effects.

According to this complex topology, one can expect a higher required number of harmonics to provide the continuity of the unsteady flow. This point is investigated below.

Influence of the Number of Harmonics on the Flow Field

Figure 13 presents the time and pitch averaged swirl at rotor exit in order to characterize the influence of the number of harmonics on the flow topology for this highly off-design point:

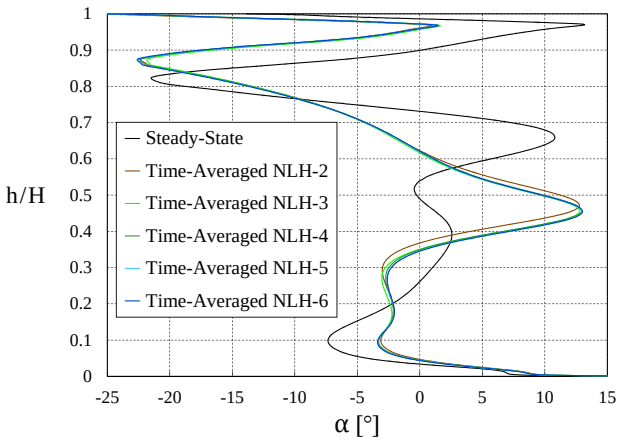

Figure 13 Evolution of the time and pitch averaged swirl at rotor exit from hub to shroud – Open stator case.

The highly distorted absolute flow angle distribution over the span is a consequence of secondary flows produced in the stage. The steady-state mixing plane result reproduces these distortions, but some discrepancies are observed in terms of amplitude and spanwise distribution compared to NLH time-averaged results. Regarding the harmonic convergence, no evolution is observed starting from 5 harmonics. This confirms previous observations related to Table 6.

To complete the approach, instantaneous entropy signals extracted at 10% span of the interface are plotted in Figure 14. A complex stator entropy signal composed by several peaks crosses the interface. Whatever the number of harmonics considered, the computation fails to capture the sharpest pic amplitude corresponding to the nozzle vane wake. This secondary flow is the most important one coming from the stator in terms of entropy creation. To catch this pic, a higher number of harmonics associated to a finer azimuthal mesh discretization would help. Although, other peaks are well captured using 5 harmonics, which seems to be a good trade-off for this operating point to keep reasonable computational resources. Similar observations arise from 50% and 90% spanwise signals. In case of mixing plane computation, the tangential averaging applied at the interface induces an important mixing loss, as the vane wake signature is present in the whole span. This explains why this configuration leads to the most important performance discrepancy between mixing plane and NLH computations (see Table 6). These flow field descriptions explain why the harmonic convergence is reached using different harmonic values for the three operating points. The a priori prediction of these numbers of harmonics might be useful to avoid such a convergence analysis. This point is discussed in the next section.

Discussion

Stator–rotor interactions

From Figures 5, 10 and 14, a focus on the entropy signal taken upstream the interface reveals an interesting interaction. The upstream signal also depends on the number of harmonics, despite the fact that only the downstream signal is recomposed. Figure 15 shows these stator entropy signals extracted at 90% span for the three operating points, from 1 to 4 harmonics. This evolution shows that some stator–rotor interactions are captured by the NLH computations. This interaction has an evolution with the number of harmonics chosen, until the harmonic convergence is reached. This is particularly true for the two off-design configurations. It might be induced by the nature of the stage since experience from designing radial turbomachinery shows that the sensibility of the stator flow to the rotor configuration is typical of radial centripetal turbines. Anyway these considerations have to be taken into account, and will directly impact the required number of harmonics. To assist this choice, a criterion has recently been proposed in [23] and is discussed in the following section.

Prediction of the number of harmonics

According to [23], if potential effects due to downstream row can be neglected, the spatial information at the interface in the stator block can be considered only. Thus mixing plane computations are adapted to provide this spatial information, leading to a cheap a priori estimation. This prediction tool is based on an azimuthal Fourier transform, which allows to calculate the cumulative energy content of a given signal up to a given harmonic (see [23] for more details). Despite the presence of potential effects discussed in the above section for the present test cases, this criterion is applied to bring a point of comparison to the previous results. These are illustrated in Table 7.

This analysis reveals that 4 harmonics are necessary for both the nominal and the closed stator case to catch 99% of the cumulative energy content. This is in good agree-

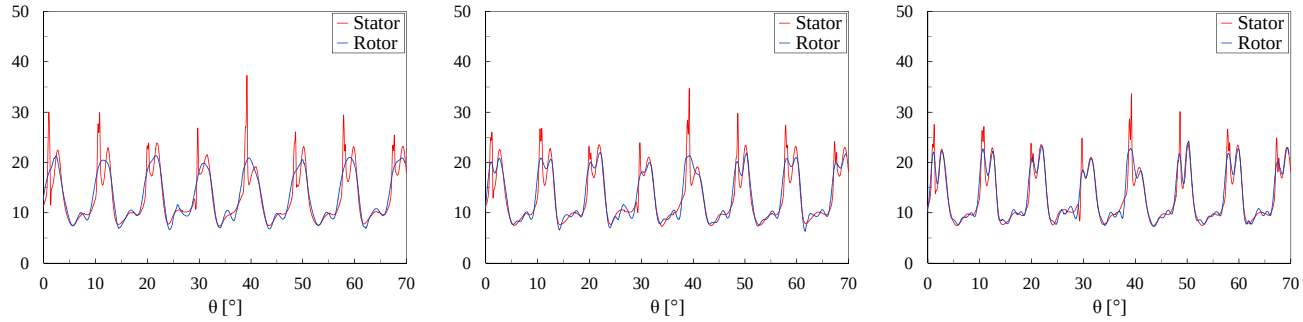

(a) 3 Harmonics (b) 4 Harmonics (c) 5 Harmonics

Figure 14 Entropy signal ($J.kg^{-1}.K^{-1}$) at the interface for the open stator case – 10% span.

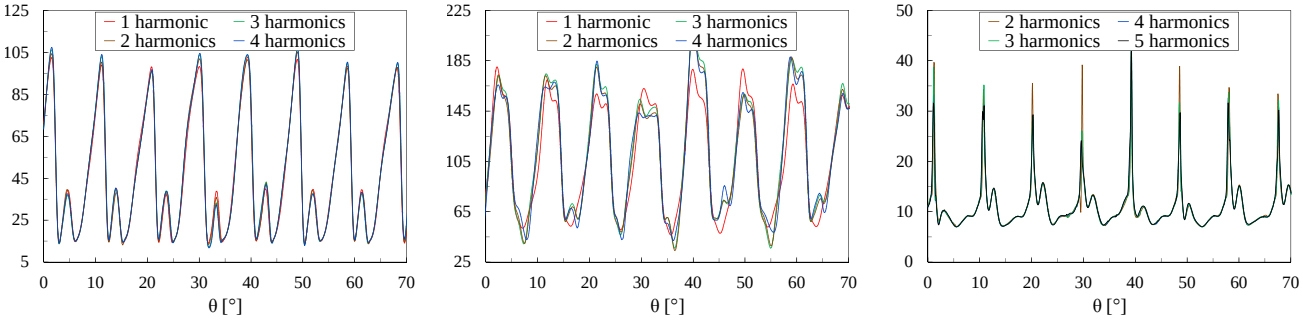

(a) Nominal point (b) Closed stator case (c) Open stator case

Figure 15 Stator entropy signal ($J.kg^{-1}.K^{-1}$) at the interface for different harmonic values – 90% span.

Table 7 Predicted number of harmonics associated to 99% of the cumulative energy content.

Operating point	Spanwise position of the signal (%)	Required number of harmonics
Nominal	10	3
	50	4
	90	3
Closed stator	10	4
	50	3
	90	4
Open stator	10	27
	50	26
	90	32

ment with both harmonic convergences led above. For the full open stator case, a major increase in the number of harmonics (32) seems necessary to catch this level of cumulative energy content. Also, according to this criteria, a NLH computation with six harmonics provides respectively 68%, 85% and 58% of the cumulative energy content at 10%, 50%, and 90% span. However, such a computation with 32 harmonics would conduct to a massive mesh size refinement to fulfil the NLH discretization requirement. The cost of such a calculation would be in the range of full annulus methods, for which the sliding mesh interface is less restrictive in terms of filtering.

Conclusions

A variable geometry radial turbine stage from Liebherr Aerospace Toulouse has been numerically investigated in this paper. Two numerical approaches are applied (mixing plane and Non Linear Harmonic) and compared for three operating conditions: the nominal point and two off-design operating points (open and closed stator). It is shown in this paper that the discrepancy between the two methods is configuration dependent, and seems to be less noticeable if nozzle endwall clearances are not included in the model. Both observations are related to the stator–rotor interactions which arise in the free space. The more sensitive the configuration is to these interactions, the more differences are recorded between the two methods (e.g. the full open stator configuration). But this difference never exceeds a few percent of the global performance prediction. For NLH computations, the harmonic convergence analysis for both the nominal and the closed stator cases are obtained using 4 harmonics. For the full open stator configuration, a value of 5 harmonics allows to reach converged performances and local flow field for the NLH time-averaged flow. However, it fails to ensure the continuity of the unsteady flow at the interface. Through the consideration of a criteria recently proposed in the literature, it seems that a value of 32 harmonics is required for the latter operating point. Though, this value cannot be considered because of meshing requirements with regard to computational resources. In addition, it is shown that the upstream unsteady signal at the interface also depends on the number of harmonics. This is a consequence of the unsteady stator–rotor interactions taken into account by the NLH approach. Thus, further works would consist in validating these results through global and local flow field exper-

imental measurements. Also, these three operating points might be studied numerically and experimentally without endwall clearance to have a complete approach of the stator clearance effects.

References

[1] Whitfield, A., and Baines, N. C., (1990), Design of Radial Turbomachines, John Wiley and Sons inc.

[2] Moustapha, H., Zelesky, M., Baines, N.C., and Japikse, D., (2003), Axial and Radial Turbines, Concepts ETI.

[3] Meitner, P. L., and Glassman, A.J., (1980), Off-Design Performance Loss Model For Radial Turbines With Pivoting, Variable Area Stators, AVRACOM Technical Report 60-C-13, NASA.

[4] Okazaki, Y., Matsudaira, N., and Hishikawa, A., (1986), A Case of Variable Geometry Turbocharger Development, I. Mech. E. Conference Publications, pages 191-195, paper 801135.

[5] Walkingshaw J. R., Spence S. W. T., Ehrard, J., and Thornhill, D., (2010), A Numerical Study of the Flow Fields in a Highly Off-Design Variable Geometry Turbine, ASME paper GT2010-22669.

[6] Putra, M. A., and Joss, F., (2006), Investigation of Secondary Flow Behavior in a Radial Turbine Nozzle, ASME paper GT2006-90019.

[7] Natkaniec, C. K., Kammeyer, J., and Seume, J.R., (2011), Secondary Flow Structures and Losses in a Radial Turbine Nozzle, ASME paper GT2011-46753.

[8] O'Neill, J. W., Spence, S. W. T., and Cunningham, G., (2005), An Assessment of Stator Vane Leakage in a Variable Geometry Radial Turbine, Proceedings of 6th European Turbomachinery Conference.

[9] Spence, S. W. T., O'Neill, J.W., and Cunningham, G. (2006), An Investigation of the Flowfield Through a Variable Geometry Turbine Stator with Vane Endwall Clearance, Proceedings of the Institution of Mechanical Engineers, Part A: Journal of Power and Energy 2006 220: 899.

[10] Tamaki, H., Goto, S., Unno, M., and Iwakami, A., (2008), The Effect of Clearance Flow of Variable Area Nozzles on Radial Turbine Performance, ASME paper GT2008-50461.

[11] Zaho, B., Yang, C., Hu, L., Sun, H., Yi, J., Eric, C., Shi, X., and Engeda, A., (2014), Understanding of the Interaction between Clearance Leakage Flow and Main Passage Flow in a VGT Turbine, Hindawi Publishing Corporation, Advances in Mechanical Engineering 7(2):652769-652769

[12] Roumeas, M., and Cros, S., (2012), Aerodynamic Investigation of a Nozzle Clearance Effect on Radial Turbine Performance, ASME paper GT2012-68835.

[13] Liu, Y., Yang, C., Qi, M., Zhang, H., Zhao, B., Shock, Leakage Flow and Wake Interactions in a Radial Turbine with Variable Guide Vanes, ASME paper GT2014-25888.

[14] Walkingshaw J. R., Spence S. W. T., and Ehrard, J., (2011), A Numerical Study of Stator Vane Tip Leakage Effects on Flow Development in a Variable Geometry Automotive Turbine, Proceedings of 9th European Turbomachinery Conference.

[15] Walkingshaw J. R., Spence S. W. T., Ehrard, J., and Thornhill, D., (2014), An Experimental Assessment of the Effects of Stator Vane Tip Clearance Location and Back Swept Blading on an Automotive Variable Geometry Turbocharger, ASME Journal of Turbomachinery, Vol. 136, No. 6, p. 061001.

[16] He, L., (2010), Fourier Methods for Turbomachinery Applications, Progress in Aerospace Sciences, Volume 46, Issue 8, November 2010, Pages 329–341.

[17] Vilmin, S., Lorrain, E., Hirsh, C., and Swoboda, M., (2006), Unsteady Flow Modeling Across the Rotor/Stator Interface Using the Nonlinear Harmonic Method, ASME paper GT2006-90210.

[18] Vilmin, S., Lorrain, E., Tartinville, B., Capron, A., and Hirsh, C., (2013), The Nonlinear Harmonic Method: from a single stage to multi-row effects, International Journal of Computational Fluid Dynamics, Volume 27, No. 2, pp. 88-99.

[19] Marlier, J., Barbieux, V., Tartinville, B., (2016), Unsteady Rotating Radial Load of a Single Stage Radial Inflow Turbine, ASME paper GT2016-56983.

[20] Kawakubo, T., (2010), Unsteady Rotor-Stator Interaction of a Radial-Inflow Turbine with Variable Nozzle Vanes, ASME paper GT2010-23677.

[21] Dufour, G., Carbonneau, X., Garcia Rosa, N., (2013), Nonlinear Harmonic Simulations of the Unsteady Aerodynamics of a Fan Stage Section at Windmill, ASME paper GT2013-95485.

[22] Sicot, F., Dufour, G., Gourdain, N., (2012), A Time-Domain Harmonic Balance Method for Rotor/Stator Interactions, ASME Journal of Turbomachinery, Vol. 134, No. 1, p. 011001.

[23] Gomar, A., Bouvy, Q., Sicot, F., Dufour, G., Cinnella, P., François, B., (2014), Convergence of Fourier-Based Methods for Turbomachinery Wake Passing Problems, Journal of Computational Physics, Vol. 278, p. 229-256.

[24] Marsan, A., and Moreau, S., (2015), Analysis of the Flow Structure in a Radial Turbine, Proceedings of 11th European Turbomachinery Conference.